Direct numerical simulation of particle-laden rotating turbulent channel flow

Yingkang Pan, Toshitsugu Tanaka, and Yutaka Tsuji[a)]
Department of Mechanophysics Engineering, Osaka University, Suita 565-0871, Japan

(Received 4 February 2000; accepted 10 May 2001)

Direct numerical simulations (DNS) of particle-laden rotating turbulent channel flows at the Reynolds number 194 and the rotation number 0.075 (both based on the friction velocity and the channel half width) on a 128^3 grid were performed. Particles were traced using the deterministic method combined with the direct particle interactions via hard-sphere collisions and two-way coupling. The particle gravity parallel to the spanwise direction and the particle volume fractions from $O(10^{-6})$ to $O(10^{-5})$ were considered. It is found that the presence of the heavier particles (Stokes number $\mathrm{St}_\tau > 0.1$) and their interparticle collisions near the pressure surface significantly changes the turbulence properties, particularly in the near-wall regions. The DNS results showed that the interparticle collisions make the lighter particle distribution more even and then attenuate the turbulence intensity of the fluid, and make the heavier particle distribution more uneven and then enhance the turbulence intensity of the fluid. It is also found that the slightly heavier particles ($\mathrm{St}_\tau = 0.126$) form strong streaky structures added ''hooks'' with a certain skew angle to the streamwise direction near the pressure surface. When the particles become larger and heavier, and the particle volume fraction becomes higher $O(10^{-5})$, the well-known low/high speed streaks near the pressure surface are destroyed by the particles due to rotation. © *2001 American Institute of Physics.* [DOI: 10.1063/1.1383790]

I. INTRODUCTION

Particle-laden flow in the rotating system is an important phenomenon in many industrial fields. In such a rotating system, particle's trajectories are greatly affected by the Coriolis and centrifugal forces, so that they considerably deviate from the streamlines of the carrier fluid. This results in a concentration gradient across the rotating channels and causes a change in the properties of the fluid and the particles. The net results are changes in the turbulence structure, its intensity, and the velocity distribution. If the particles are of an erosive nature, the impact of the particles on surfaces can cause severe erosion damage. Engineering applications are even more numerous; to mention a few: gas turbines operating with working fluids containing solid particles, induced fans for cleaning the ducts in a room.

For the single-phase rotating channel flow, it is well known that the spanwise rotation affects both the mean motion and the turbulence structure. Bradshaw[1] pointed out the similarity among rotation, streamline curvature, and thermal stratification on turbulent flows and defined an equivalent gradient ''Richardson number'' to identify either a stabilizing or destabilizing effect on the flow subject to system rotation. It was formally demonstrated by Johnston *et al.*[2] by considering simplified forms of the transport equations for the individual components of the Reynolds stress tensor. This essential issue has been elaborated by Tritton[3] and Cambon *et al.*[4] The single-phase turbulent rotating flow at a low Reynolds number has been studied in detail by means of the direct numerical simulation (DNS) by Kristoffersen and Andersson.[5] They used a 128^3 grid and the finite-difference method. Their DNS results showed that, with increasing rotation, the augmentation and damping of the turbulence along the pressure and suction surfaces, respectively, became more significant, resulting in highly asymmetric profiles of mean velocity and turbulent Reynolds stresses; the vortices were shifted slightly towards the pressure surface with increasing rotation rates, and the number of vortex pairs therefore tend to increase with the rotation number $\mathrm{Ro}_\tau = \Omega H/u_\tau$. Their DNS on the rotating shear flows reproduced many of the experimentally observed effects of the Coriolis forces on the mean flow and its turbulence structure.

Particle-laden rotating turbulent channel flows are extremely difficult to be observed experimentally in detail, even given today's sophisticated laser measurements. Until now, DNS of the Navier–Stokes equations is the most accurate computational approach to the problem, since all essential scales of turbulent motions are resolved. In the present simulations, the dispersed particles were traced using the deterministic method based on the equations of motion and rotation which are exact within certain formal limits containing the Coriolis and centrifugal forces. The interaction between the instantaneous velocity field and the particle motion is described completely. Hard-sphere collision model based on the impulsive force which is defined by the integral of the force acting on a particle versus time was applied to account for the particle interactions. Therefore, the present simulation should supply data, which are a representation with high resolution of the motions of small particles in a rotating tur-

a)Author to whom correspondence should be addressed. Electronic mail: tsuji@mech.eng.osaka-u.ac.jp

bulent channel flow and its effects on turbulence. The advantage over experimentation is that detailed data are available for analysis, although the present simulations are limited to the low Reynolds number.

McLaughlin[6] and Brooke *et al.*[7,8] used the DNS technique contributing to the understanding of the mechanism of particle deposition in aerosols, showing that particles accumulate in the near-wall region. Pedinotti *et al.*[9] have shown that particles tend to segregate into the low-speed region of the fluid motion near the wall and are subsequently resuspended by ejection from the wall in horizontal channels. Rouson and Eaton[10] performed DNS of particle-laden channel flows; they found that heavy particles tend to disperse uniformly and light particles form clusters. Many DNS results have been performed in isotropic turbulence and have shown that particles with relaxation time of the order of the Kolmogorov time scale are preferentially concentrated into regions of low vorticity and high strain rate (e.g., see Squires and Eaton,[11] Wang and Maxey[12]). Elghobashi and Truesdell[13] applied the DNS technique to model particle dispersion in decaying homogeneous and isotropic turbulence. Very recently, Ling *et al.*[14] performed DNS of a three-dimensional temporal mixing layer with particle dispersion, and found the mushroom shape of particle distribution. On the other hand, Pan and Banerjee[15] conducted DNS with large particles and investigated the effects of large particles on wall turbulence.

In recent studies,[16–18] the interparticle collision statistics of small particles was performed by applying DNS to the isotropic turbulence with collision kernels. It was found that particles with small Stokes number behave similarly to the prediction of Saffman and Turner,[19] and on the other hand, particles with very large Stokes numbers have collision frequencies similar to the kinetic theory of Abrahamson.[20] Very recently, Sundaram and Collins[21] conducted DNS of isotropic turbulence by suspended particles considering the particle interactions with hard-sphere collision model; they found a novel two-field formalism to calculate two-point correlations and equivalent spectral densities. Yamamoto *et al.*[22] performed the large-eddy simulation (LES) of the particle-laden vertical channel flows with the hard-sphere collision model, and found that the interparticle collisions affect the particle distributions and turbulence near the walls.

There exist few investigations on the particle-laden flows in rotating channels. The group of Tabakoff[23] performed experimental and analytical investigations concerning the effects of the presence of solid particles on the performance of turbomachines. But, they had not considered the interparticle collisions and the effects of particles on the fluid turbulence. In our previous work,[24] we conducted the LES of particle-laden rotating channel flows, and found that small and light particles accumulate near the pressure surface; interparticle collision frequency is very high near the pressure surface even at a very low averaged volume fraction $O(10^{-5})$; the effect of the small and light particles is to attenuate the contribution from the Coriolis forces to the turbulence structure and the total turbulent kinetic energy of the carrier fluid, particularly near the walls. Until now, the effects of the small particles on wall–turbulence and the interparticle, particle–wall collisions on turbulence structure near walls due to system rotation have not been very clear.

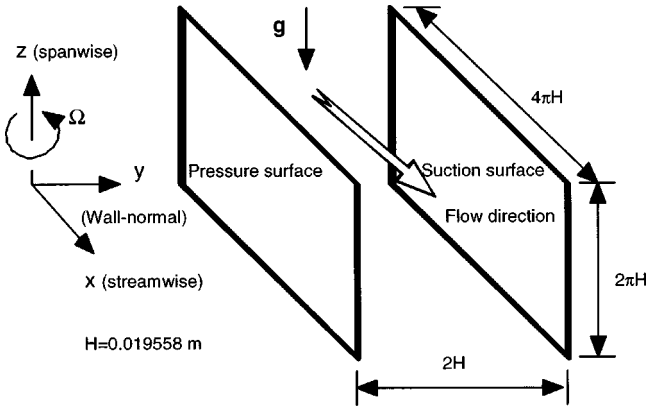

FIG. 1. Flow geometry and coordinate system.

The objective of the present work is to investigate the three-dimensional patterns of particles, interparticle collisions, and particle–turbulence interactions in developed rotating turbulent channel flows based on our previous work.[24] A primary interest of this study is to determine the utility of DNS for prediction of particle concentration and interparticle collision effects on the fluid turbulence. The DNS results also can provide the database for establishing subgrid stress modeling in the large eddy simulation of particle-laden rotating turbulent flows.

II. SIMULATION OVERVIEW

A. Fluid field

Figure 1 illustrates the coordinate system used to write the equations of motion. The pressure-driven turbulent flow between two infinite parallel plates in spanwise rotation with constant angular velocity about the z axis is considered here. Here, x or x_1 is the streamwise direction, y or x_2 is the wall-normal direction, and z or x_3 is the spanwise direction. Also, u or u_1 is the streamwise velocity, v or u_2 is the velocity in the wall-normal direction, and w or u_3 is the velocity in the spanwise direction. Periodic boundary conditions are applied both in the streamwise x- and spanwise z directions.

The turbulent flows in a rotating channel were calculated using DNS of the incompressible continuity and the Navier–Stokes equations, which can be expressed in a relative coordinate system (x,y,z) in the following dimensionless forms:

$$\frac{\partial u_j}{\partial x_j}=0, \tag{1}$$

$$\frac{\partial u_i}{\partial t}+\frac{\partial}{\partial x_j}(u_i u_j)=-\frac{\partial p_{\mathrm{eff}}}{\partial x_i}+\frac{1}{\mathrm{Re}_\tau}\frac{\partial^2 u_i}{\partial x_j \partial x_j}+2\delta_{i1}+2\varepsilon_{ij3}\mathrm{Ro}_\tau u_j+F_{pi}, \tag{2}$$

where δ_{ij} is the Kronecker delta symbol; ε_{ijk} is the Levi–Civita's alternating tensor.

The third term on the right-hand side in Eq. (2) is the dimensionless, gross downstream pressure gradient which

would maintain a steady flow against the equilibrium and long-term wall friction produced by both boundaries. F_{pi} in Eq. (2) is the local average of the reaction of fluid force on particles, in the x_i direction, exerted per unit mass of fluid. In the present simulations, F_{pi} is evaluated by

$$F_{pi} = -\frac{1}{\rho}\sum_{n=1}^{N} F_{n,i}, \tag{3}$$

where n indicates a particle number and N is the instantaneous number of particles, $N=N(x_1,x_2,x_3,t)$, in the cell at which Eq. (2) is calculated. $F_{n,i}$ is the instantaneous nondimensionalized force acting on a particle n. If we do the one-way coupling simulation, $F_{n,i}$ is set to zero. The fourth term on the right-hand side in Eq. (2) is the Coriolis force experienced by a fluid element resulting from system rotation. The centrifugal force has a conservative nature and can be combined with the pressure gradient term

$$p_{\text{eff}} = p - \tfrac{1}{2}\mathrm{Ro}_\tau^2 r^2, \tag{4}$$

where p is the normalized static pressure and r denotes the dimensionless distance from the axis of rotation. Equation (2) is nondimensionalized by the time-averaged mean wall friction velocity ($u_\tau = \sqrt{\tau_w/\rho}$) and the channel half-width (H). Based on this normalization, the Reynolds number is defined as $\mathrm{Re}_\tau = u_\tau H/\nu$, and the Rotation number as $\mathrm{Ro}_\tau = \Omega H/u_\tau$, where Ω is the angular velocity of rotation. In a stationary channel flow without rotation, the time-averaged mean wall friction velocities are the same on both walls of the channel, but this is not the case with rotation because of the asymmetry introduced by the Coriolis forces. If we define the time-averaged friction velocity on the stable and unstable sides of the channel as $u_{\tau s}$ and $u_{\tau u}$, respectively, then the following relationship can be obtained:

$$u_\tau^2 = \tfrac{1}{2}(u_{\tau s}^2 + u_{\tau u}^2). \tag{5}$$

The governing Eqs. (1) and (2) were solved numerically using a semi-implicit method. The divergence form (2) we used is conservative for finite-difference schemes when a staggered grid is used. Spatial derivatives were approximated by a second-order accuracy central difference scheme. The advancement scheme for the velocity components u_i is a compact-storage third-order Runge–Kutta scheme published by Spalart *et al.*[25] which has an explicit treatment for the convective terms and the source terms including the particle's feedback, and second-order-implicit Crank–Nicolson for the viscous term. This semi-implicit scheme seems more suitable for the present cases because of their stability and is regarded as a standard scheme in the direct numerical simulation. An approximate factorization technique in three directions combined with the fractional step procedure (Kim and Moin[26]) is used to get the prediction values of velocities. The fully developing flow under consideration is driven by an imposed mean pressure gradient, in the x direction, so that the turbulence may be treated as homogeneous in the streamwise-(x) and spanwise (z) directions, i.e., mean properties and turbulence statistics vary only in the y direction normal to the plates. Therefore, the Poisson equation for pressure was solved using Fourier series expansions in the streamwise and spanwise directions together with tridiagonal matrix inversion.

B. Particle motion

Although the mass loading ratio is on the order of unity, the particle volume fraction is still very low for most particle-laden rotating channel flows, especially in turbomachines. Many particles accumulate near the pressure surface (unstable side) because of the Coriolis forces. Therefore, the interparticle collisions (including particle–wall collisions) are very important in such flows, and should be considered (Pan *et al.*[24]). The influence of the particles on the flow field and its turbulence structure is little known, so from the present DNS results, we get some detailed information concerning this phenomenon.

Motion of a small rigid sphere in a turbulent flow field is described by a complicated equation by Maxey and Riley.[27] If all particles are rigid spheres with identical diameter d_p and density ρ_p, and the density of the particles is much larger than that of the carrier fluid, the equation of particle motion can be simplified in a rotating frame of reference with the axis of rotation aligned with the spanwise direction. It can be given in the following dimensional form:

$$m_p\frac{du_{pi}}{dt} = \frac{1}{2}\rho|\mathbf{u}_R|A\left[C_D\mathbf{u}_{Ri} + C_{LR}\frac{(\mathbf{u}_R\times\boldsymbol{\omega}_R)_i}{|\boldsymbol{\omega}_R|}\right] + f_{LG}\delta_{i2} - m_p g\,\delta_{i3} + \delta_{i1}m_p\Omega^2 r + 2\varepsilon_{ij3}m_p\Omega u_{pj}, \tag{6}$$

where m_p is the mass of a particle, u_{pi} the velcity of the particle in the x_i direction, ρ the density of the fluid, and A the projected area of the particle. $\mathbf{u}_\mathrm{R}$ and $\boldsymbol{\omega}_\mathrm{R}$ are, respectively, the relative velocity and rotation velocity vectors of the particle with respect to the fluid. The last two terms in Eq. (6) are the centrifugal force and the Coriolis force, respectively. Unlike the carrier fluid, the centrifugal force of the particle has no conservative nature. Those two extra forces enhance the interparticle and particle–wall collisions and affect the particle's performance. The empirical relation for C_D (Schiller and Naumann[28]) was employed, as

$$C_D = \frac{24}{\mathrm{Re}_p}(1 + 0.15\,\mathrm{Re}_p^{0.687}), \tag{7}$$

where Re_p is the particle Reynolds number defined as $\mathrm{Re}_p = d_p|\mathbf{u}_R|/\nu$, in which $\boldsymbol{\nu}$ is the kinematic viscosity of the carrier fluid. Rubinow and Keller[29] derived the formula of the lift force developed due to rotation of the particle for Reynolds numbers at the order of unity. The lift force due to rotation of the particle for Reynolds numbers greater than 1.0

TABLE I. Coefficients of particle rotation.

Re_R	C_{T1}	C_{T2}	C_{T3}
$\mathrm{Re}_R<1$	0.0	16π	0.0
$1<\mathrm{Re}_R<10$	0.0	16π	0.0418
$10<\mathrm{Re}_R<20$	5.32	37.2	0.0
$20<\mathrm{Re}_R<50$	6.44	32.2	0.0
$50<\mathrm{Re}_R<100$	6.45	32.1	0.0

is still an open question. In the present simulations of the particle-laden rotating channel flows, the lift forces are much smaller than the drag force and the gravity. The particle Reynolds number for the most simulated particles is greater than 1.0. For the larger particles, the particle Reynolds number is greater than 10.0 frequently due to system rotation. In the present simulations, we employed the lift coefficient C_{LR} in the following form:[30]

$$C_{LR}=\min\left(0.5,\ 0.25\frac{d_p|\boldsymbol{\omega}_R|}{|\mathbf{u}_R|}\right). \tag{8}$$

Saffman[31,32] derived the formula of the lift force due to the velocity gradient on a particle for Reynolds numbers much less than unity. The experiments of Hall[33] showed that the predictions of Saffman are near the experimental data for the particle Reynolds number larger than 6 in a turbulent boundary layer. In addition, Tanaka and Tsuji[34] found that the simulations considering the Saffman lift force had a good agreement of particle density distribution in a vertical pipe with their experimental data. So, the Saffman lift force is considered here. In the present simulations, periodic bound-

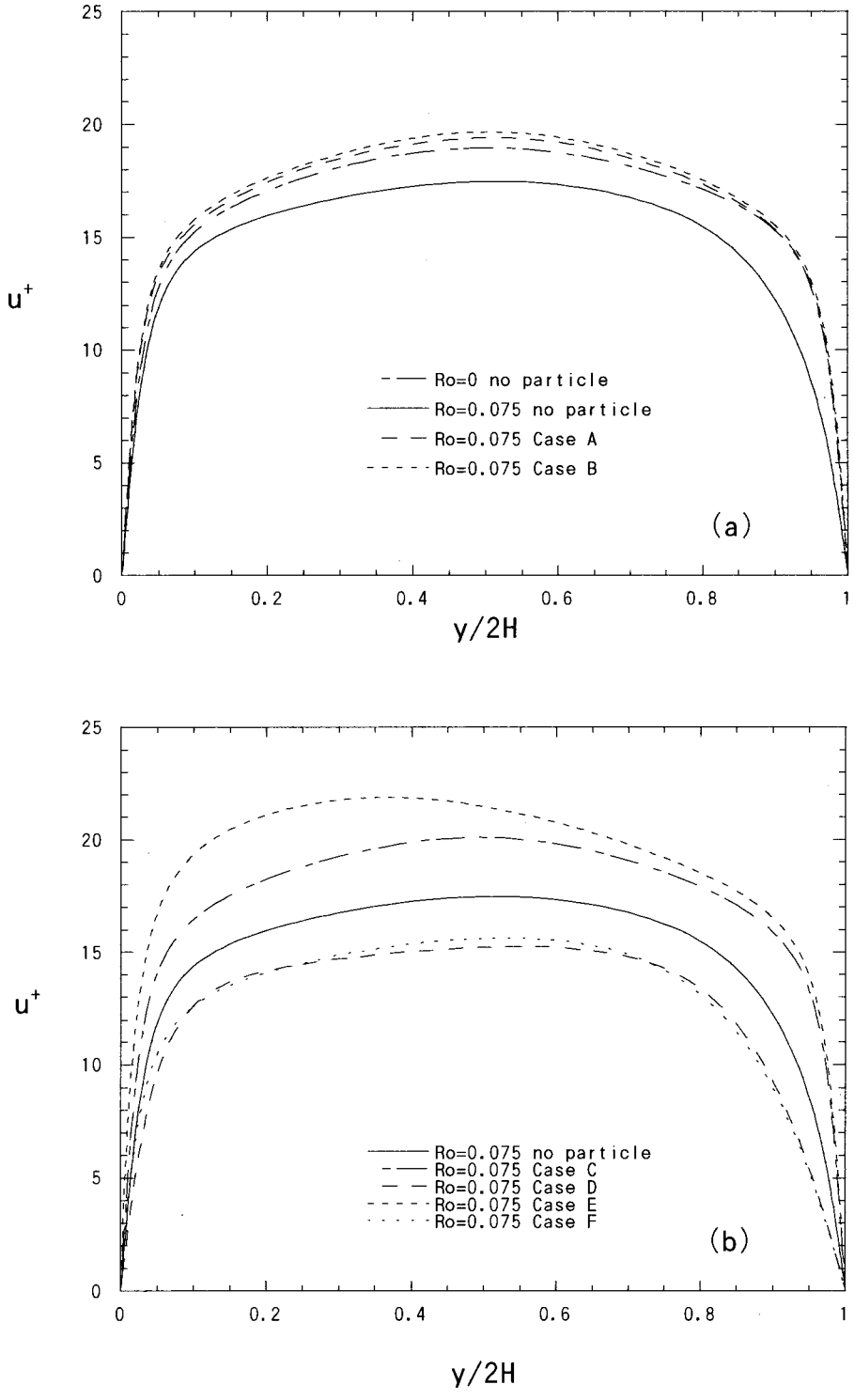

FIG. 2. Mean streamwise velocity distribution of the fluid, u^+, in global coordinates. (a) Cases A and B; (b) Cases C, D, E, and F.

ary conditions were applied both in streamwise and spanwise directions. Therefore, the mean velocity gradients in those two directions can be regarded as negligibly small. The Saffman lift force was employed only in the wall-normal component with the expression as following:

$$f_{LG} = -1.61 d_p^2 \rho u_{Rx} \sqrt{\nu \left| \frac{\partial u_{Rx}}{\partial y} \right|} \frac{\partial u_{Rx}/\partial y}{|\partial u_{Rx}/\partial y|}. \tag{9}$$

The equation of rotational motion of a particle is given by

$$I \frac{d\omega_{pi}}{dt} = -C_T \frac{1}{2} \rho \left(\frac{d_p}{2} \right)^2 |\boldsymbol{\omega}_R| \omega_{Ri}, \tag{10}$$

where I is the moment of inertia of a particle. The right-hand side of Eq. (9) is the viscous torque against the particle's rotation, which is theoretically obtained by Dennis *et al.*[35] and Takagi.[36] C_T is the nondimensional coefficient determined by the rotational Reynolds number, $\mathrm{Re}_R = d_p^2 |\boldsymbol{\omega}_R| / 4\nu$. It can be expressed as

$$C_T = \frac{C_{T1}}{\sqrt{\mathrm{Re}_R}} + \frac{C_{T2}}{\mathrm{Re}_R} + C_{T3} \mathrm{Re}_R. \tag{11}$$

The coefficients of C_{T1}, C_{T2}, and C_{T3} are determined by Re_R. When $\mathrm{Re}_R < 10$, we applied the values of C_{T1}, C_{T2}, and C_{T3} by Takagi.[36] When $\mathrm{Re}_R > 10$, we applied the values of C_{T1}, C_{T2}, and C_{T3} by Denis *et al.*[35] This is summarized in Table I. The momentum response time τ_p is the time for momentum transfer due to drag and is calculated from

$$\tau_p = \left(\frac{4 d_p}{3 C_D} \right) \left(\frac{\rho_p}{\rho} \right) \frac{1}{|u_i - u_{pi}|} = \frac{d_p^2}{18\nu} \frac{\rho_p}{\rho} \frac{1}{(1 + 0.15\, \mathrm{Re}_p^{0.687})}. \tag{12}$$

In the present simulations, the mean slip velocity between the fluid and the particles is applied in calculating the momentum response time τ_p. The Stokes number St_τ of the particles is defined as the ratio of the particle's momentum response time to the time scale of the carrier fluid

$$\mathrm{St}_\tau = \frac{\tau_p}{H/u_\tau}. \tag{13}$$

Many time scales exist in the rotating turbulence flow. In the present simulations, the nondimensional time unit (H/u_τ) is employed for simplicity. The translational velocity and the rotation velocity of a particle can be obtained by integrating Eqs. (6) or (9) using the second-order Adams–Bashforth explicit scheme, respectively. The position of a particle can be gotten according to velocity

$$u_{pi}^{(n+1)} = u_{pi}^{(n)} + \frac{\Delta t}{2} (3 H_{upi}^{(n)} - H_{upi}^{(n-1)}), \tag{14}$$

$$\omega_{pi}^{(n+1)} = \omega_{pi}^{(n)} + \frac{\Delta t}{2} (3 H_{\omega pi}^{(n)} - H_{\omega pi}^{(n-1)}), \tag{15}$$

$$x_{pi}^{(n+1)} = x_{pi}^{(n)} + \frac{\Delta t}{2} (u_{pi}^{(n)} + u_{pi}^{(n+1)}), \tag{16}$$

where $H_{upi}, H_{\omega pi}$ are the sums of all terms in the right-hand sides of Eqs. (6) and (10), respectively. In the present simulations, a three-dimensional 8-node Lagrangian interpolation polynomial was used to obtain the velocities of the carrier fluid at the positions of the particles.

C. Interparticle collision

Interparticle collisions take an important role in the flow field near the pressure surface in the particle-laden rotating channels due to the particle concentration. In the present

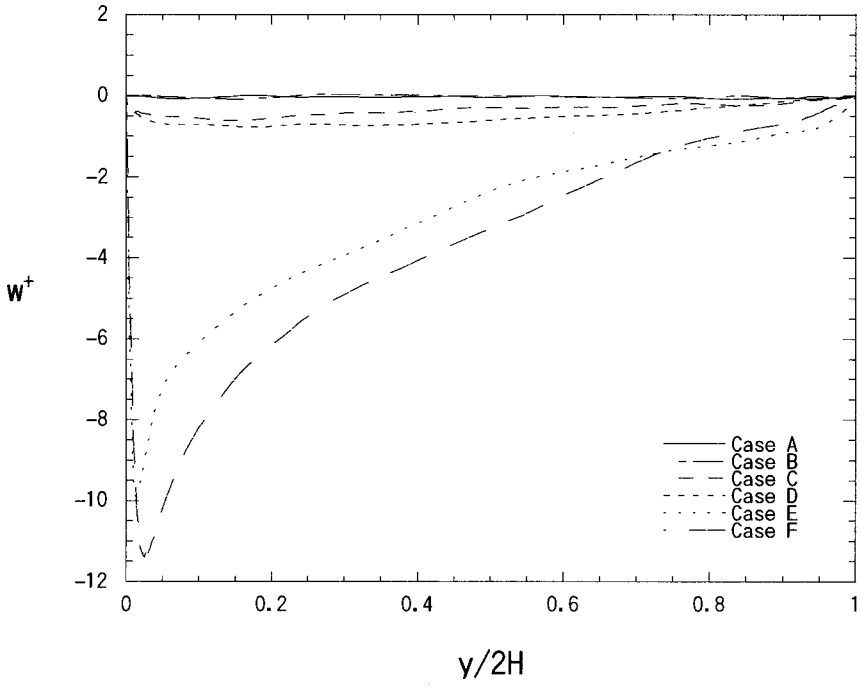

FIG. 3. Mean spanwise velocity distribution of the fluid, w^+, in global coordinates, Ro=0.075.

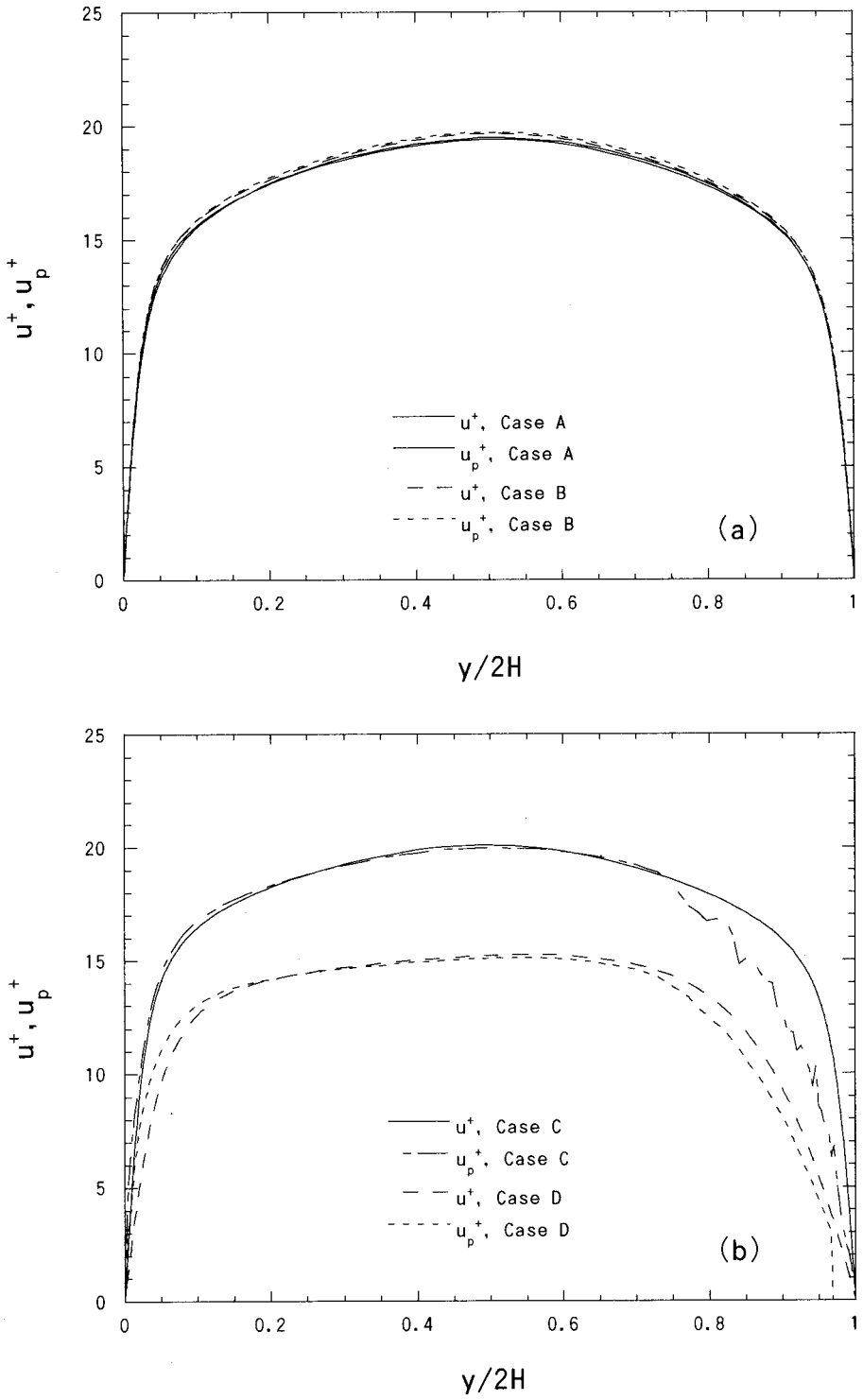

FIG. 4. Mean streamwise velocity distribution of the fluid and the particles, u^+ and u_p^+, in global coordinates, Ro=0.075. (a) Cases A and B; (b) Cases C and D.

situations, particle number density is so low that we used the deterministic method (Tanaka and Tsuji[34]). It is assumed that the particle volume fraction is so small that the binary collisions dominate in our cases. Therefore, collision is mainly detected by calculating the distance of two particles' centers at the specific time when two particles collide with each other. Postcollision motion of the particle is described by the equations of impulsive motion as

$$u_{pi}^* = u_{pi} + \frac{\mathbf{J}}{m_p}, \tag{17}$$

$$u_{pj}^* = u_{pj} - \frac{\mathbf{J}}{m_p}, \tag{18}$$

$$\omega_{pi}^* = \omega_{pi} + \frac{d_p}{2}\mathbf{n}\times\frac{\mathbf{J}}{I}, \tag{19}$$

$$\omega_{pj}^* = \omega_{pj} + \frac{d_p}{2}\mathbf{n}\times\frac{\mathbf{J}}{I}, \tag{20}$$

where $\mathbf{J}$ is the impulsive force exerting on the particle i and $\mathbf{n}$ is the normal unit vector directing from the center of the

particle i to the contacting point. u_{pi}^* and u_{pj}^* are the postcollision velocities. ω_{pi}^* and ω_{pj}^* are the postcollision rotation velocities. Based on assuming spherical particles, a constant coefficient of restitution e and negligible particle deformation are assumed. **J** is given by Tanaka and Tsuji[34] in following forms:

$$\mathbf{J}=J_n\mathbf{n}+J_t\mathbf{t}, \tag{21}$$

$$J_t=\min\left[-\mu_p J_n, \frac{M}{7}|\mathbf{c}_s|\right], \tag{22}$$

$$J_n=(1+e)M\mathbf{c}\cdot\mathbf{n}, \tag{23}$$

where **t** is the tangential unit vector of the slip velocity from the particle j to the particle i, e is the coefficient of restitution, μ_p is the coefficient of friction. M is equal to m_p for

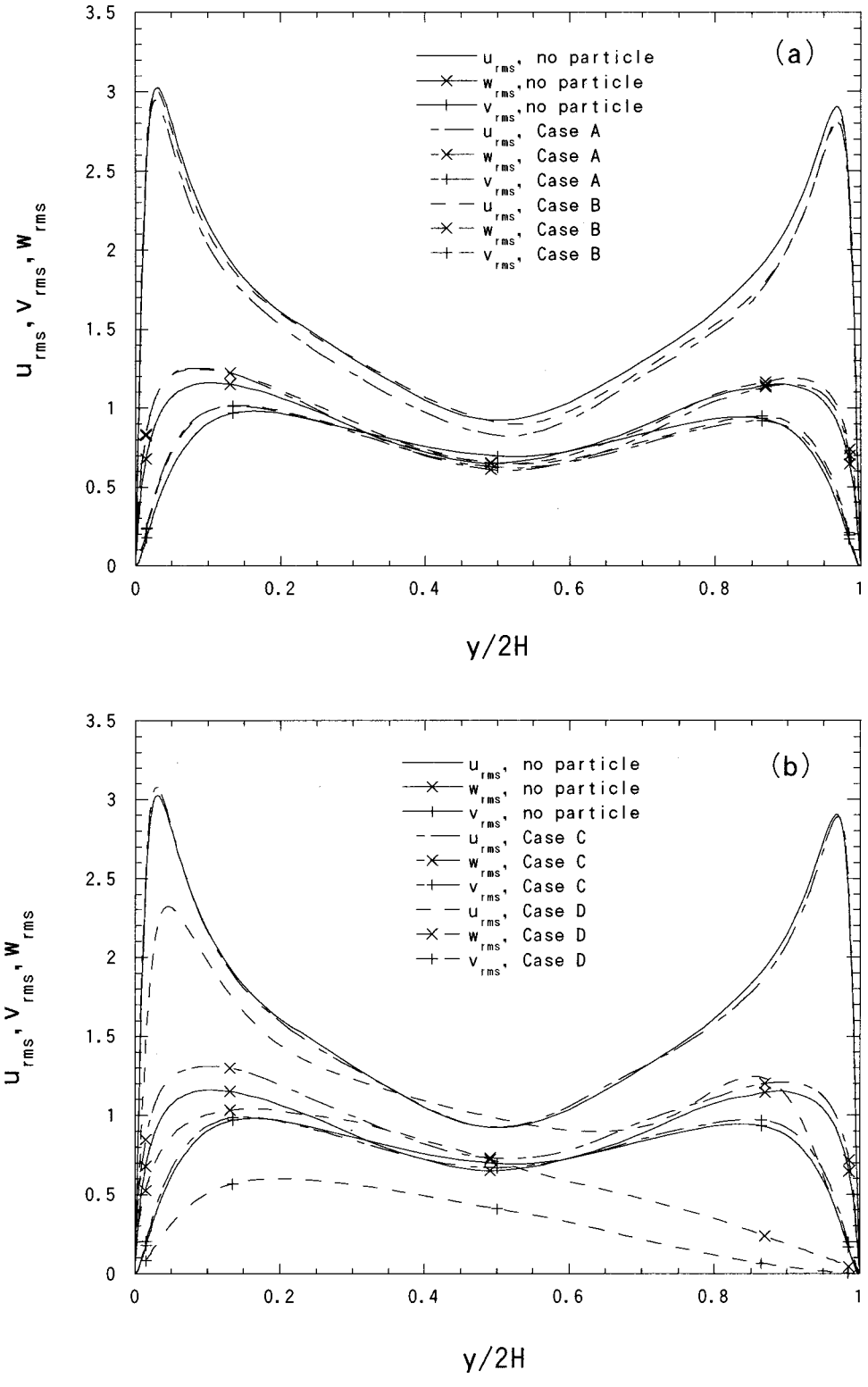

FIG. 5. Root-mean-square values of the velocity fluctuations of the fluid distribution (u_{rms}/u_τ, v_{rms}/u_τ, and w_{rms}/u_τ) comparison among different cases in global coordinates, Ro $=0.075$. (a) Cases A and B; (b) Cases C and D; (c) Cases E and F.

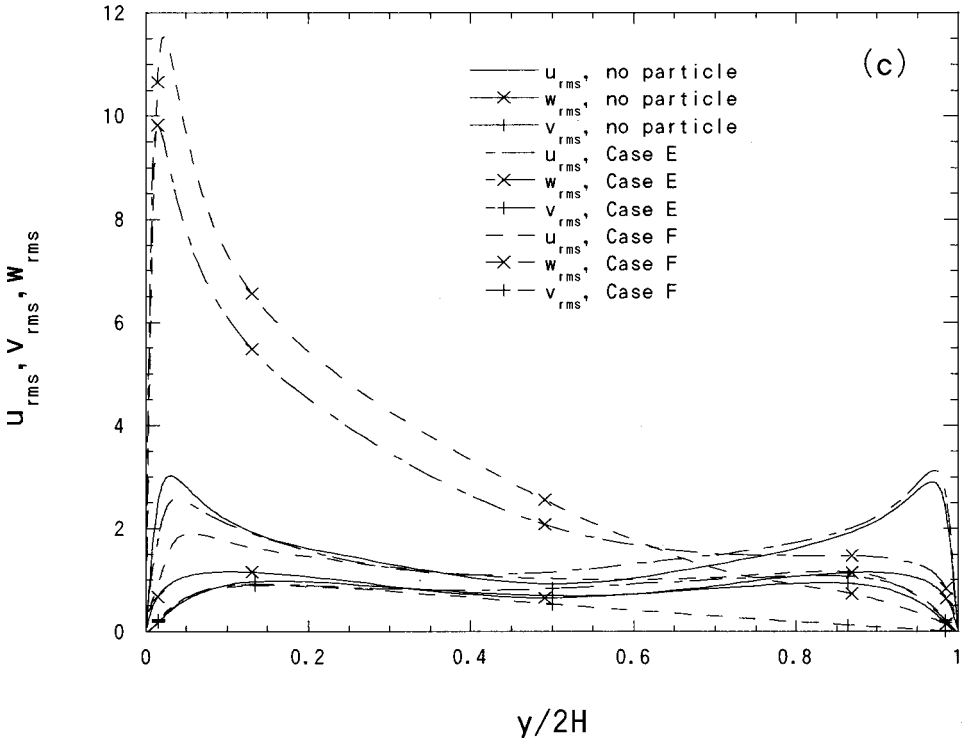

FIG. 5. (*Continued.*)

interparticle collisions and $2m_p$ for particle–wall collisions. **c** is the relative velocity of mass center, and c_s is the slip velocity at the contact point.

III. RESULTS AND DISCUSSION

The initial conditions of velocity fluctuations of the fluid and the particles were assumed by a generator of random number, and the particle's initial velocities were assumed to be the same as the fluid velocities at the particle positions. The initial mean velocity along the y direction is assumed to the minimum of $y^+ = yu_\tau/\nu$ and semilogarithmic law distribution, $U^+ = \min(y^+, 2.5 \ln y^+ + 5.5)$. In all the numerical experiments the calculation domain used was $4\pi H \times 2H \times 2\pi H$ in x, y, and z directions, respectively, which is same as that used by Kim *et al.*[37] The calculation domain was divided into 128^3 computational cells with a uniformly spaced grid in the x- and z directions ($\Delta x^+ = 19.046$, $\Delta z^+ = 9.523$) and a nonuniform grid distribution in the y direction

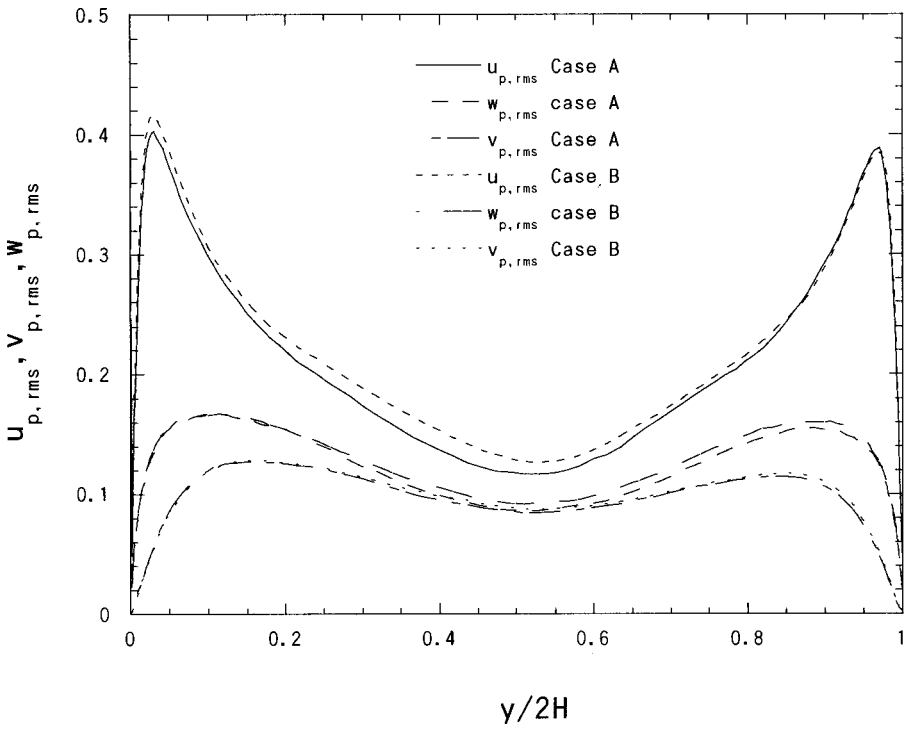

FIG. 6. Root-mean-square values of the particle velocity fluctuations distribution ($u_{p,\mathrm{rms}}/u_\tau$, $v_{p,\mathrm{rms}}/u_\tau$, and $w_{p,\mathrm{rms}}/u_\tau$) comparison between case A and case B in global coordinates, Ro $=0.075$.

TABLE II. Particle properties for different cases.

Case	$d_p(\mu\text{m})$	Material	ρ_p (kg/m^3)	$\phi_v(10^{-6})$	ϕ	τ_p(ms)	St_τ	Interparticle collisions
A	28	Lycopodium	700	1.52	0.0009	1.63	0.124	Yes
B	28	Lycopodium	700	1.52	0.0009	1.58	0.0120	No
C	50	Glass	2500	8.65	0.0181	16.6	0.126	Yes
D	50	Glass	2500	8.65	0.0181	16.8	0.128	No
E	70	Copper	8800	23.74	0.1741	88.6	0.674	Yes
F	70	Copper	8800	23.74	0.1741	90.1	0.685	No

($\Delta y^+_{\text{min}}=0.292$, $\Delta y^+_{\text{max}}=7.104$) for $\text{Re}_\tau=194$. The Reynolds number of the single-phase flow, based on the bulk mean velocity U_m (about 2.22 m/s) and the channel half-width H, was about 2900. In the present simulations a hyperbolic tan-

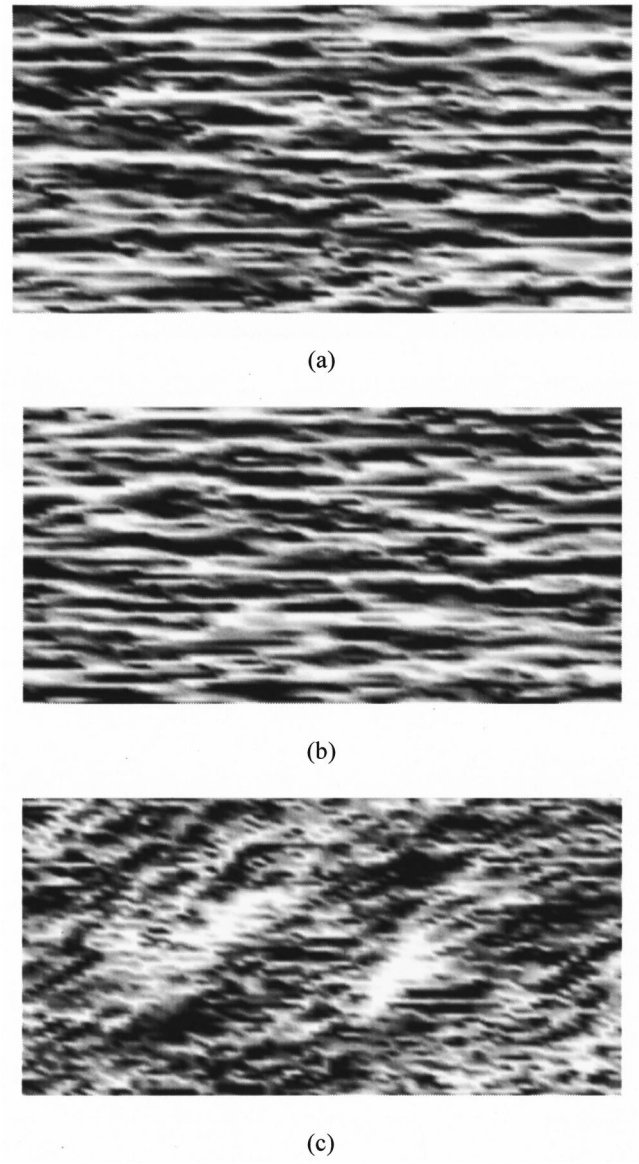

FIG. 7. Instantaneous streamwise velocity fluctuation distribution near the pressure surface ($y^+=11.08$) at time 8 H/u_τ. (a) Case A; (b) Case C; (c) Case E.

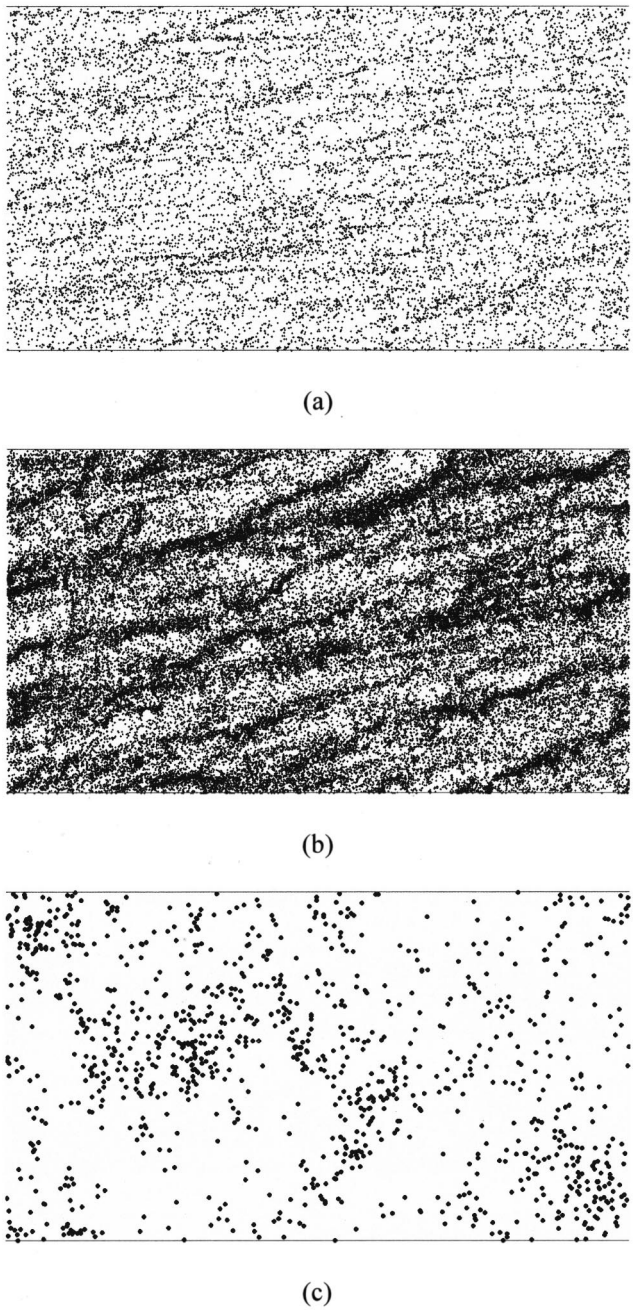

FIG. 8. Instantaneous particle distribution structures near the pressure surface at time 8 H/u_τ. (a) Case A, $y^+<0.47$; (b) Case C, $y^+<0.47$; (c) Case E, $y^+<1.17$.

gent transformation is used to generate the grid in the y direction. In the present simulations, the computational domain is far from the axis of rotation. The inlet rotation radius of the domain is set to be large enough, $r_0 = 50.41H$, where $H = 0.019\,558m$, so that the computational domain is located in the experimental area of Johnston *et al.*[2] Based on the above assumptions, periodic boundary conditions in the x- and z directions for both the fluid and the particles were employed in the present simulations.

In the present study, we investigate the modification of turbulence in rotating channel flows due to the particles and system rotation, with emphasis on the near-pressure and suction wall regions. The simulations are done for cases with different particles, diameters, and volume fractions. Particle properties of different cases are listed in Table II, in which ϕ_v is the averaged volume fraction of the particles, ϕ is the averaged mass loading ratio of the particles, and the value of τ_p is based on the averaged particle Reynolds number for the corresponding case. The averaged particle Reynolds numbers are 0.154 for case A, 0.334 for case B, 1.119 for case C,

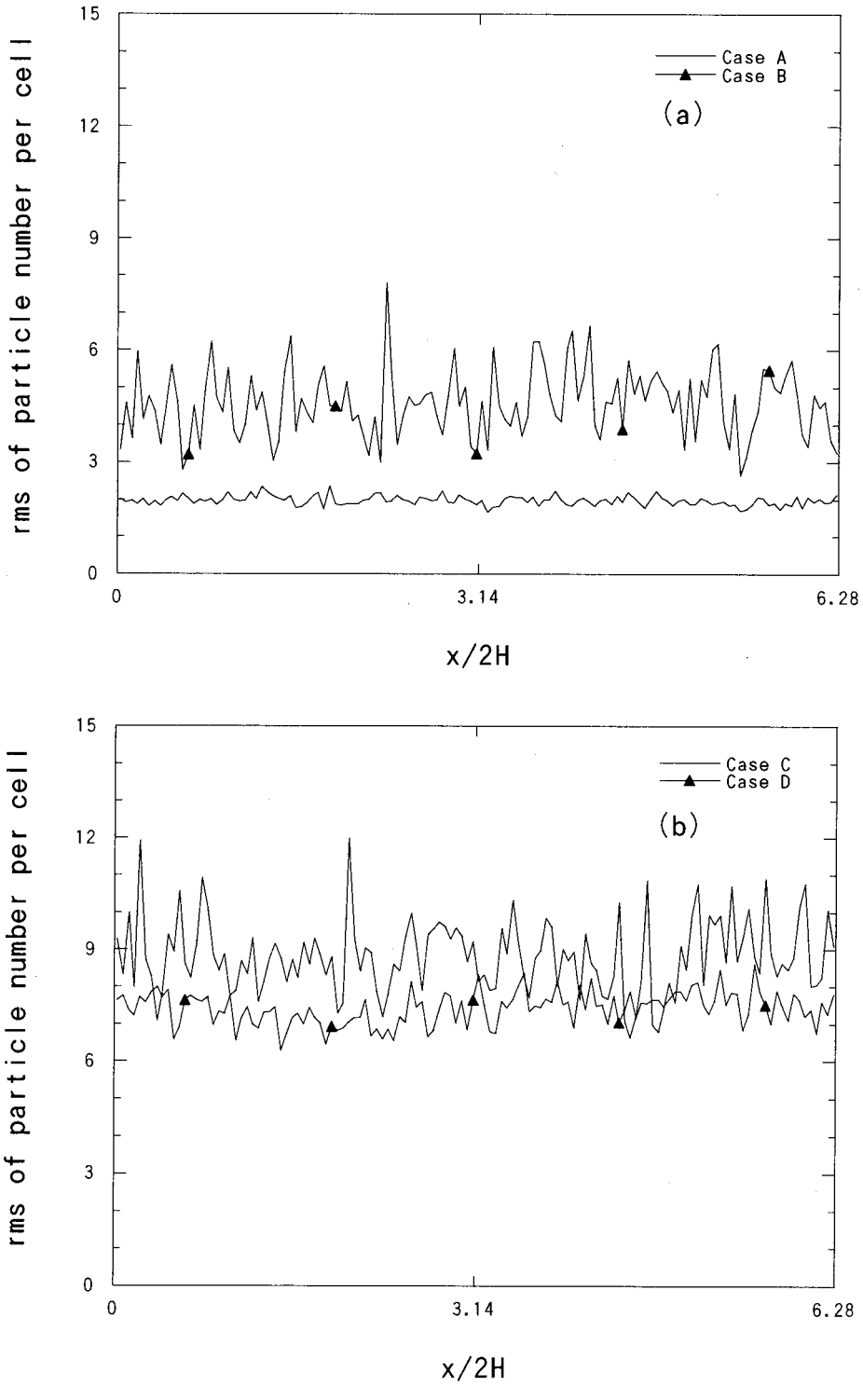

FIG. 9. Comparison of $N_{\mathrm{rms}}(x)$ for the particles at time $8\,H/u_\tau$. (a) Cases A and B; (b) Cases C and D; (c) Cases E and F.

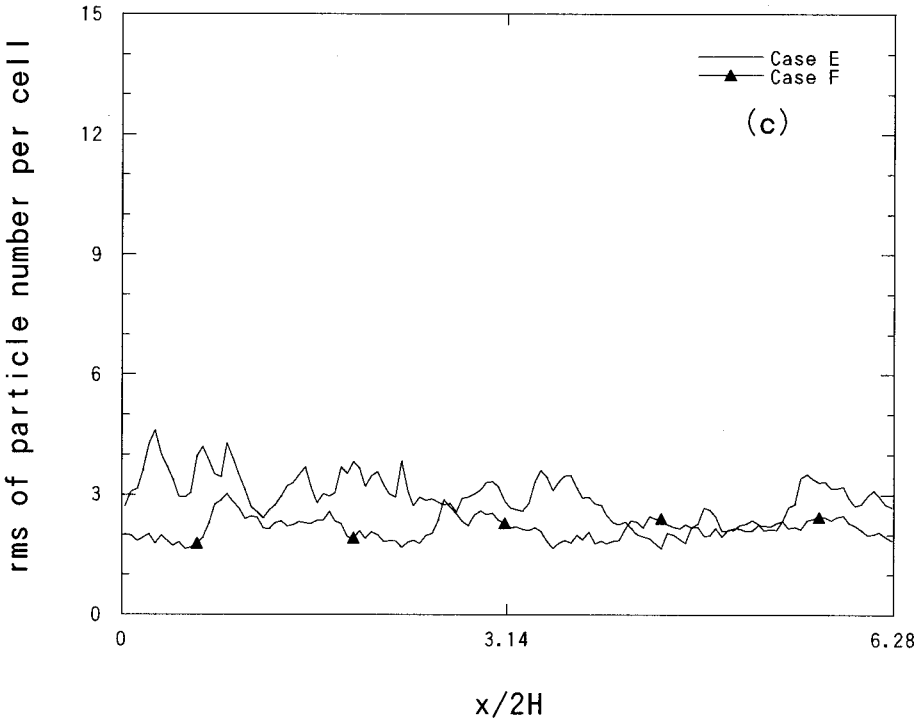

FIG. 9. (*Continued.*)

0.948 for case D, 5.80 for case E, and 5.39 for case F, respectively. All of the simulated cases in Table II have the same particle number $N_p = 156\,159$. Cases A, C, and E have been considered the interparticle collisions with a hard-sphere model. On the contrary, cases B, D, and F have not been considered the interparticle collisions. Considering the interparticle collisions, the dispersed particles are simulated in dimensionalized units. So, the fluid is assumed as air with the properties ($\nu = 1.5\times10^{-5}\,\mathrm{m^2/s}$, $\rho = 1.2\,\mathrm{kg/m^3}$). The time step used in all the cases was 0.0008 nondimensional time units (H/u_τ) for the fluid and the particle motion and 0.004 for the interparticle collisions. These are much smaller than the particle momentum response time τ_p, and so the particle motion can be assumed linear during one time step period. Before we start to simulate the particle-laden flows, a fully developed rotating channel flow field must be prepared. First, to get the fully developed nonrotating channel turbulent flow field not influenced by the initial conditions, the flow field was advanced up to 28 nondimensionalized time units. The simulated mean averaged values and the turbulence intensities agreed well with the results of spectral method of Kim *et al.*[37] After that the fully developed rotating channel flow field at the rotation number 0.075 was obtained by conducting the DNS in another 12 nondimensional time units (H/u_τ). Second, each case of the particle-laden rotating channel flows listed in Table II was performed in another 8 H/u_τ to reach the fully developed particle-laden rotating channel flow. Almost all parts of the program for the fluid were vectorized. In the rest of the paper, the Reynolds number and rotation number Re_τ, Ro_τ are referred to as Re and Ro for notational simplicity.

A. Particle effects on mean properties

The mean streamwise velocity profile of the fluid nondimensionalized by the wall–shear velocity obtained from the present DNS is shown in Fig. 2. Figure 2 shows that the mean streamwise velocity $u^+ = u/u_\tau$ of the single-phase flow of rotation becomes smaller than the one without rotation. The stabilization of turbulence near suction surface ($y/2H = 1.0$) is reflected in reduced velocity gradients, while near pressure surface ($y/2H = 0.0$), the increased turbulence production causes steeper velocity gradients. The DNS results of Kristoffersen and Andersson[5] also showed this phenomenon. From Figs. 2(a) and 2(b), we can see that different particles have different effects on the mean streamwise velocity distributions of the fluid. Smaller and lighter particles (Lycopodia, cases A and B) enhance the mean streamwise velocity of the fluid; their interparticle collisions attenuate slightly the mean streamwise velocity of the fluid. For larger and heavier particles (cases C, D, E, and F), their interparticle collision effects are very obvious. The mean streamwise velocity with interparticle collision model is much greater than that without it at the very low particle volume fractions $O(10^{-5})$, especially for the case of copper particles in the region near the pressure surface. Figure 3 compares the mean spanwise velocity $w^+ = w/u_\tau$ profiles of the fluid obtained from different cases at the same rotation number $\mathrm{Ro} = 0.075$ in global coordinates. The gravity is parallel to the minus z coordinate. As expected, the spanwise velocity of the fluid is nearly zero for smaller and lighter particles. For larger and heavier particles (cases E and F), the spanwise velocities of the fluid have peak values of -9.91 at $y^+ = 6.17$ and -11.4 at $y^+ = 11.9$ near the pressure surface, respectively. They have a steep velocity gradient in the region near the pressure surface. The interparticle collisions of glass or copper particles attenuate the absolute spanwise velocity of the fluid.

Figure 4 shows the comparison of the mean streamwise velocity distributions in global coordinates between the fluid and the particles (u^+ and $u_p^+ = u_p/u_\tau$) of different cases at

the rotation number 0.075. For smaller and lighter particles (Lycopodia, cases A and B) at the low volume fractions $O(10^{-6})$, the mean streamwise velocity difference between the fluid and the particles is very small. For glass particles (cases C and D) at the higher volume fractions $O(10^{-5})$, the mean streamwise velocity of the particles is almost same as the fluid's in the center area of the rotating channel. The particle's streamwise velocity becomes larger near the pressure surface and smaller near the suction surface than the fluid's. It is seen that the particles are more sensitive to the Coriolis and centrifugal forces than the fluid.

B. Particle effects on turbulence intensities

Comparison of turbulence intensities [root-mean-square (rms) values of velocity fluctuations] normalized by the wall-shear velocity, $u_{\mathrm{rms}}=\sqrt{\overline{u'^2}}/u_\tau$, $v_{\mathrm{rms}}=\sqrt{\overline{v^2}}/u_\tau$, and $w_{\mathrm{rms}}=\sqrt{\overline{w^2}}/u_\tau$, between the cases with and without interparticle

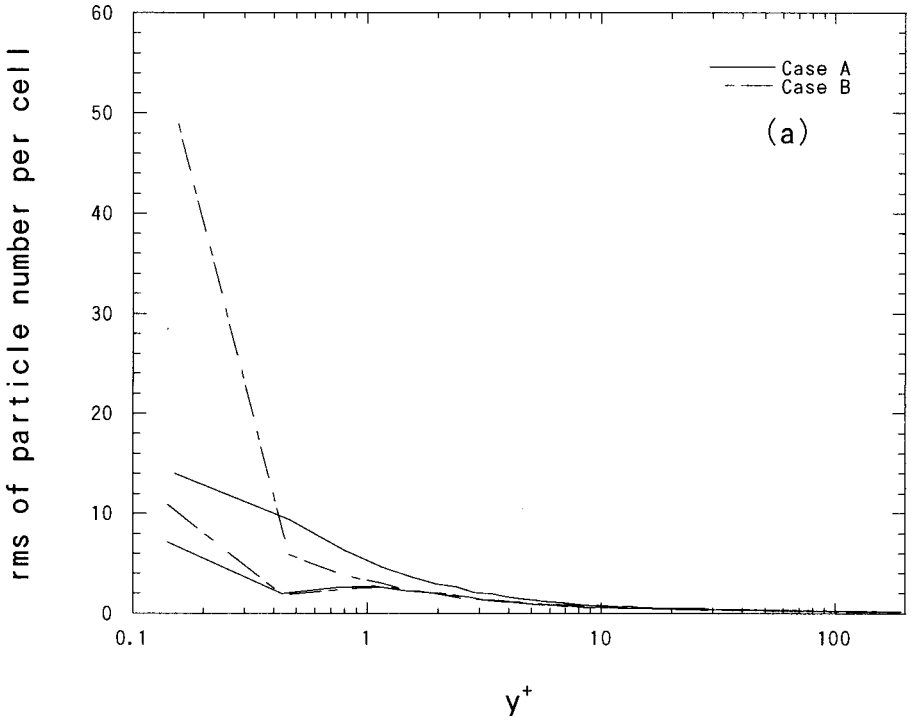

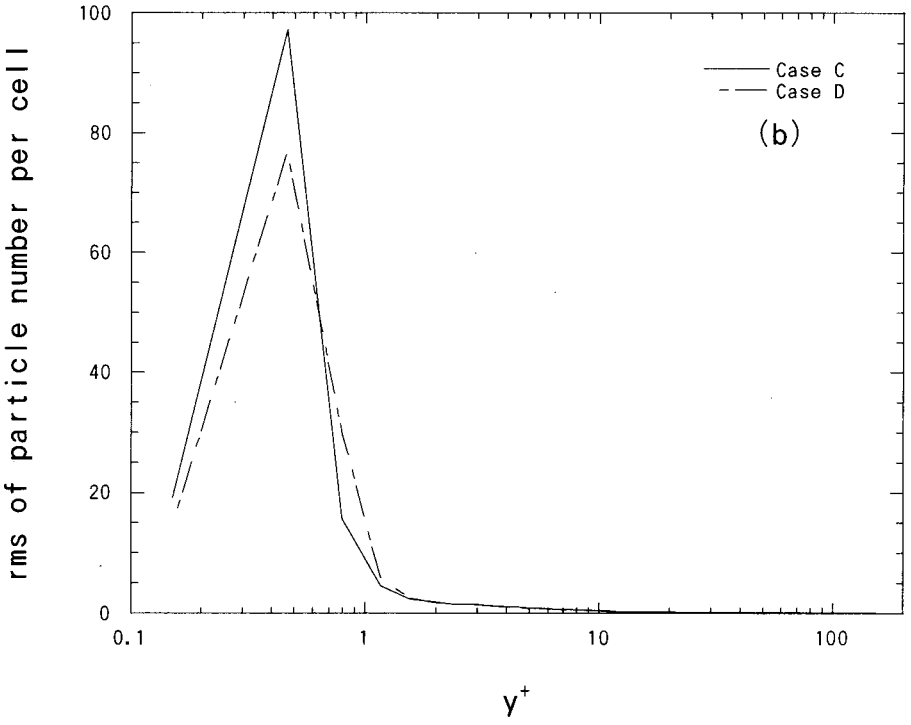

FIG. 10. Comparison of $N_{\mathrm{rms}}(y)$ for the particles in wall coordinates at time $8\,H/u_\tau$. (a) Cases A and B; (b) Cases C and D; (c) Cases E and F.

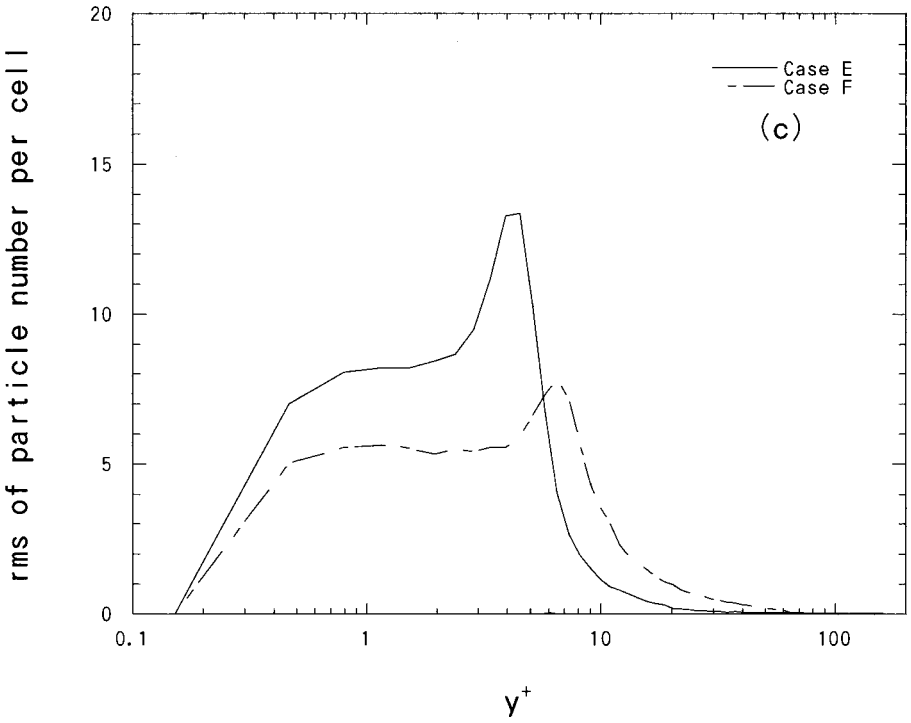

FIG. 10. (*Continued.*)

collisions is shown in Fig. 5. For smaller and lighter particles [Lycopodia, cases A and B in Fig. 5(a)], the effect of interparticle collisions is to slightly attenuate the turbulence intensities of the carrier fluid in all three directions. The streamwise fluctuations are well predicted with peak values of 2.946 at $y^+=10.95$ near the pressure surface and 2.806 at $y^+=11.22$ near the suction surface to case A. So, the stabilization/destabilization of turbulence on walls normal to the axis of rotation can be observed. For larger and heavier particles [glass and copper particles in Figs. 5(b) and 5(c)], the difference between the cases with and without interparticle collisions becomes very large. For the cases without interparticle collisions, significant attenuation of turbulence intensities in three directions is observed in whole regions except for the cases of the copper particles in the spanwise direction. The interparticle collisions significantly enhance the turbulence intensities in three directions, particularly in the region near the suction surface, except for the cases of the copper particles in the spanwise direction. Copper particles with diameter $d_p=70\,\mu$m affect not only the mean spanwise velocity but also its fluctuations significantly. Their interparticle collisions attenuate velocity fluctuations in the spanwise direction. The streamwise fluctuations are predicted with peak values of 2.576 at $y^+=16.69$ near the pressure surface and 3.127 at $y^+=10.36$ near the suction surface to the case E. However, the total turbulent kinetic energy in the region near the pressure surface is much larger than that in the region near the suction surface subjected rotation.

Figure 6 shows the comparison of particle's statistic turbulence intensities $u_{p,\mathrm{rms}}=\sqrt{\overline{u_p'^2}}/u_\tau$, $v_{p,\mathrm{rms}}=\sqrt{\overline{v_p^2}}/u_\tau$, and $w_{p,\mathrm{rms}}=\sqrt{\overline{w_p^2}}/u_\tau$, between the cases with and without interparticle collisions. Because of the heavier particle concentration very close to the pressure surface, it is very difficult to get their statistic values. In the present simulations, only the lycopodium particles with the diameter $d_p=28\,\mu$m were calculated. For smaller and lighter particles, slight attenuation of the root-mean-square (rms) values of the particle velocity fluctuations can be observed in three directions due to the interparticle collisions. The particle's velocity fluctuations are much smaller than the fluid's because of weak rotation and gravity.

In our recent study,[38] it was found that in a rotating system the turbulence modulation due to the existence of particles is related to the ratio of the rotation time scale $[1/(2\Omega)]$ to the particle momentum response time τ_p, $\mathrm{Ro}_p=1/(2\Omega\tau_p)$. The fluid–particle exchange rates of kinetic energy and dissipation can be obviously detected when Ro_p is small. In the present DNS simulations, the rotation time scale $[1/(2\Omega)]$ keeps constant 0.877 s for all the cases, the averaged values of τ_p for the different cases are shown in Table II. For the cases with the glass or copper particles, the values of Ro_p are much smaller than those of the cases with the lycopodium particles. Therefore, the effects of particles on turbulence modulation are significant and can be detected for the cases with the glass or copper particles.

It is known that the slip velocity between the fluid and the particle becomes larger when the particles are larger and heavier. Because of particle concentrations near the pressure surface, the effect of the particles through the force term is to have an explicit contribution to the Reynolds stress budget for the larger and heavier particles in this area. The dissipation and viscous diffusion are changed consequently near the pressure surface. Interparticle collisions modify the particle instantaneous velocity and then affect the particle distributions. Therefore, the effect of interparticle collisions is to suppress or enhance the fluid turbulence.

C. Particle effects on turbulent flow structures

To obtain the particle effects on turbulence structure, we set the observing $x-z$ plane near the pressure surface at $y^+ = 11.08$, where the rms values of the turbulent fluctuations are near their maximums. The instantaneous streamwise velocity fluctuation distributions in the observing $x-z$ plane at eight nondimensional time units (H/u_τ) are shown in Fig. 7. In those continuous gray scale contours, the white part expresses lower velocity area and the black one expresses higher velocity area. The structures for cases A and C with the same particle number are similar both near the pressure and suction surfaces; those cases form well-known low/high speed streaks [Figs. 7(a) and 7(b)]. The structures for cases E and F in the observing $x-z$ plane are very different from others. The well-known low/high speed streaks are totally destroyed. The area becomes much larger than other cases. The structure near the suction surface of the case E also has been changed; the streaky structures are reserved but not

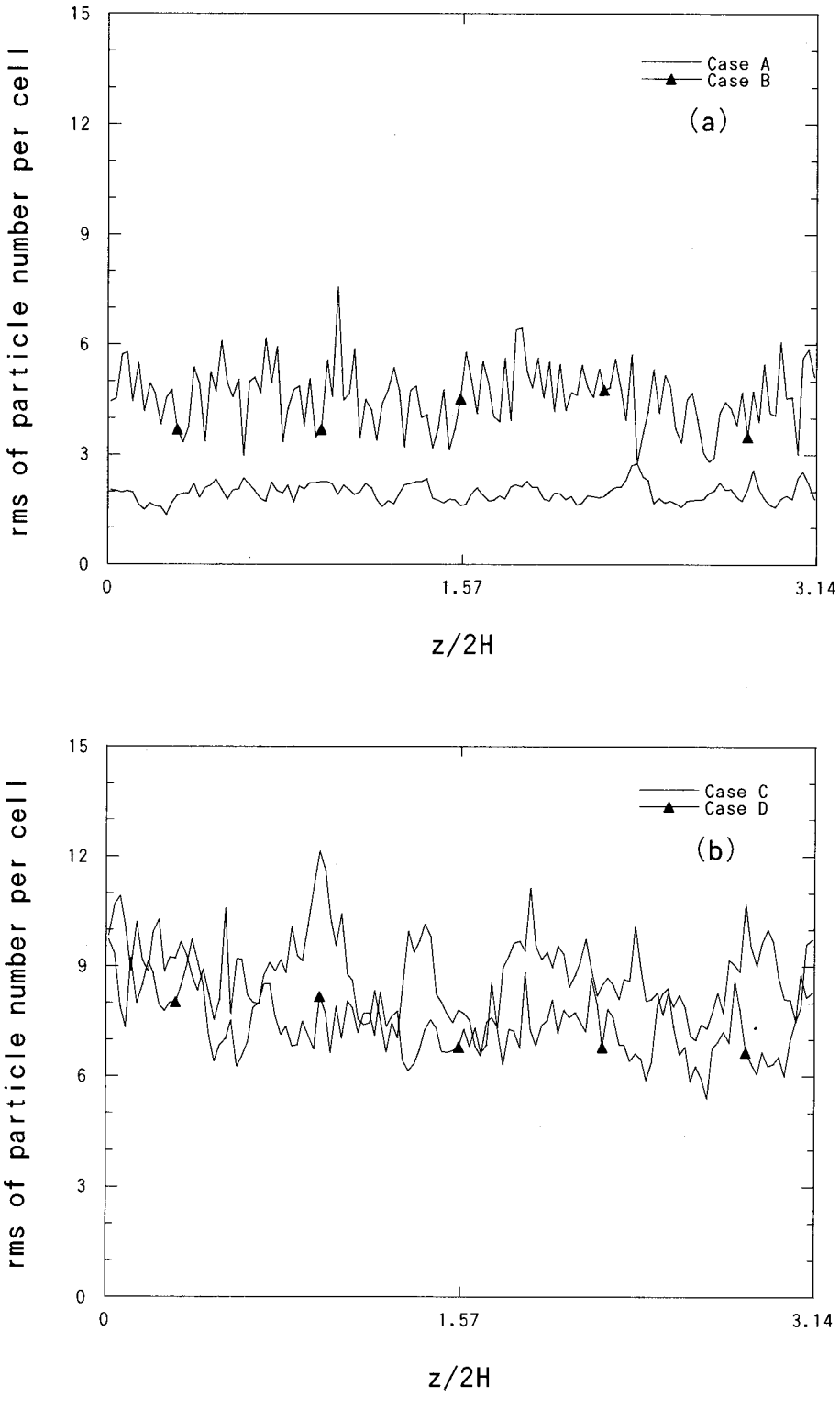

FIG. 11. Comparison of $N_{\mathrm{rms}}(z)$ for the particles at time 8 H/u_τ. (a) Cases A and B; (b) Cases C and D; (c) Cases E and F.

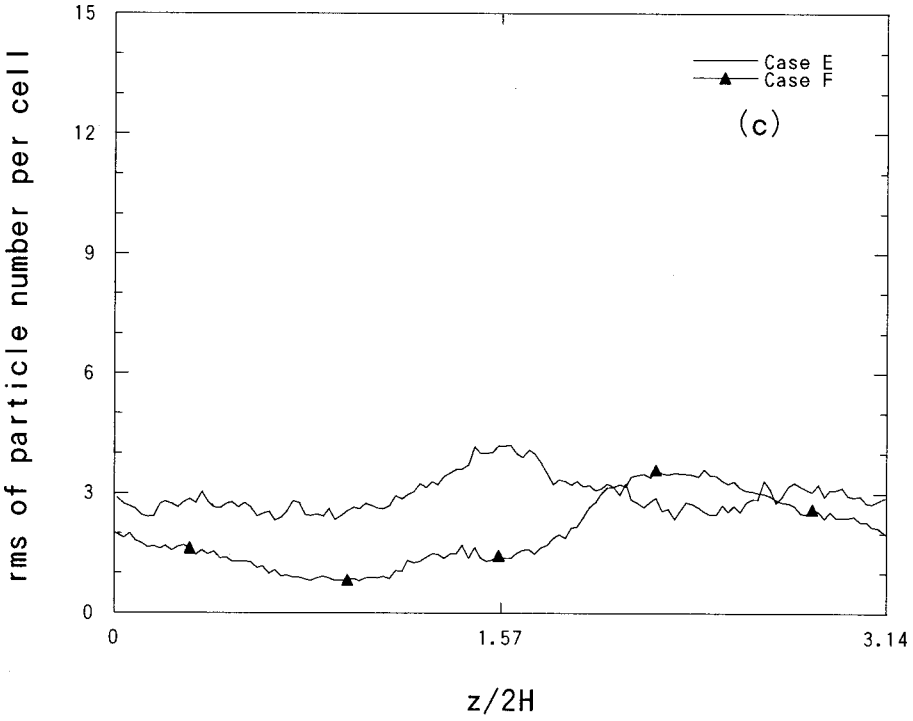

FIG. 11. (*Continued.*)

strictly parallel to the streamwise direction. It can be seen that particle concentration near the pressure surface affects the instantaneous streamwise velocity fluctuation distributions of the fluid in different ways near two walls.

D. Preferential concentration

It is known from our previous work (LES results[24]) that small and light particles (Lycopodia with the diameter $d_p = 28\,\mu$m) accumulate in the region near the pressure surface in a rotating channel. The particle density distributions are changed by high interparticle collision frequency in the region near the pressure surface subjected to rotation at the low particle volume fractions $O(10^{-5})$. From the present DNS results, more detailed and precise structures can be observed. Figure 8 shows the ''snapshot'' particle distribution near the pressure surface at eight nondimensional time units (H/u_τ). As expected, lycopodium particles with diameter $d_p = 28\,\mu$m form streaky structures similar to those found by Rouson and Eaton[10] using the DNS technique in nonrotating channel particle-laden flows [Fig. 8(a)]. In contrast, glass particles with diameter $d_p = 50\,\mu$m form a strong streaky structures with added ''hooks'' with about 15 degrees skew angle to the streamwise direction [Fig. 8(b)]. The hooks are probably due to gravity of the particles. Fewer copper particles with diameter $d_p = 70\,\mu$m concentrate in the region very close to the pressure surface [Fig. 8(c)]. This phenomenon may be caused by both the ''burst'' event and their larger inertia in interparticle and particle–wall collisions.

A quantitative comparison of the particle concentrations can by made by introducing the root-mean-square values of particle number per cell for each plane (Ling *et al.*[14])

$$N_{\mathrm{rms}}(x_i) = \left(\sum_{j=1}^{n_{cp}} (N_j(x_i) V_{c,m}/V_{c,j})^2 / N_{cp} \right)^{1/2}, \qquad (24)$$

where N_{cp} is the total number of computational cells in each plane and $N_j(x_i)$ is the number of particles in the jth cell in that plane, $V_{c,m}$ is the mean cell volume, and V_{cj} is the jth cell volume. x_i $(i=1,2,3)$ means the streamwise, cross-stream, and spanwise directions, respectively. With a uniform computational cell, Eq. (24) is exactly the same as one defined by Ling *et al.*[14] Figures 9, 10, and 11 show the comparisons of $N_{\mathrm{rms}}(x)$, $N_{\mathrm{rms}}(y)$, $N_{\mathrm{rms}}(z)$ for three kinds of particles between the cases with and without interparticle collisions. From the figures, it is seen that interparticle collisions make the smaller and lighter particle distributions $(\mathrm{St}_\tau = 0.0124)$ more even in all three directions. In contrast, they make the larger and heavier particle distributions (Stokes numbers St_τ equal to 0.126, 0.674, respectively) more uneven. Compared with the interparticle collision effects on turbulence intensities, it can be seen that the interparticle collisions make the smaller and lighter particle distributions more even and then attenuate the turbulence intensities of the fluid, and make the larger and heavier particle distributions more uneven and then enhance the turbulence intensities of the fluid. From the figures, we also can see that the $N_{\mathrm{rms}}(x_i)$ values of glass particles (cases C and D) are much greater than the ones of lycopodium particles (cases A and B) and copper particles (cases E and F). The intensities of streamwise streaky structures of the particles can be quantitatively obtained from the averaged values in Figs. 11(a) and 11(b). The highest $N_{\mathrm{rms}}(z)$ values reach 2.77 at $z/2H = 2.344$ for case A and 12.14 at $z/2H = 0.945$ for case C. The preferential concentration of the particles near the pressure surface due to rotation can be obtained quantitatively from Fig. 10. For the larger and heavier particles (cases C, D, E, and F), almost no particles accumulate near the suction surface. The highest $N_{\mathrm{rms}}(y)$ values reach 14.02

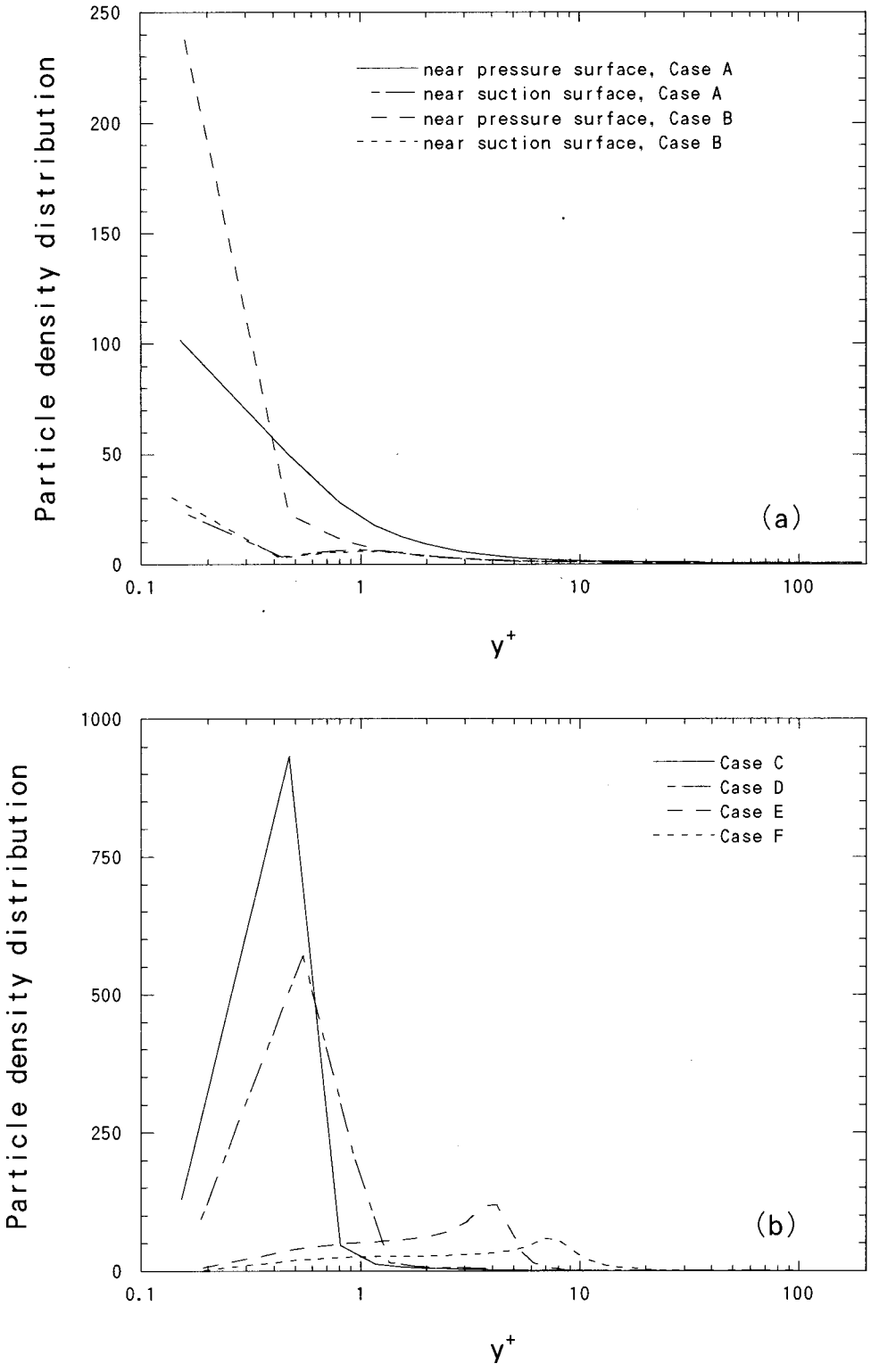

FIG. 12. Mean particle density distributions, $\phi_{y,v}/\phi_v$, in wall coordinates. (a) Lycopodium particles near both surfaces; (b) glass and copper particles near the pressure surface.

at $y^+=0.151$ for case A, and 97.2 at $y^+=0.468$ for case C, and 13.4 at $y^+=4.8$ for case E near the pressure surfaces, respectively.

The particle density distributions, $\phi_{y,v}/\phi_v$, near the surfaces in wall coordinates are shown in Figs. 12(a) and 12(b), where $\phi_{y,v}$ is the particle volume fraction with conventional averages over the streamwise- and spanwise directions and in time. From the simulation results, it is found that many particles accumulate in the vicinity of the pressure surface, and few lycopodium particles remain near the suction surface due to rotation. There are almost no glass and copper particles near the suction surface. For the cases with lycopodium and glass particles, it is also found that many particles are located in the inner boundary layer $y^+<5$. The effects of the interparticle collisions on the particle density distribution are different for cases of various particles. For the case B not con-

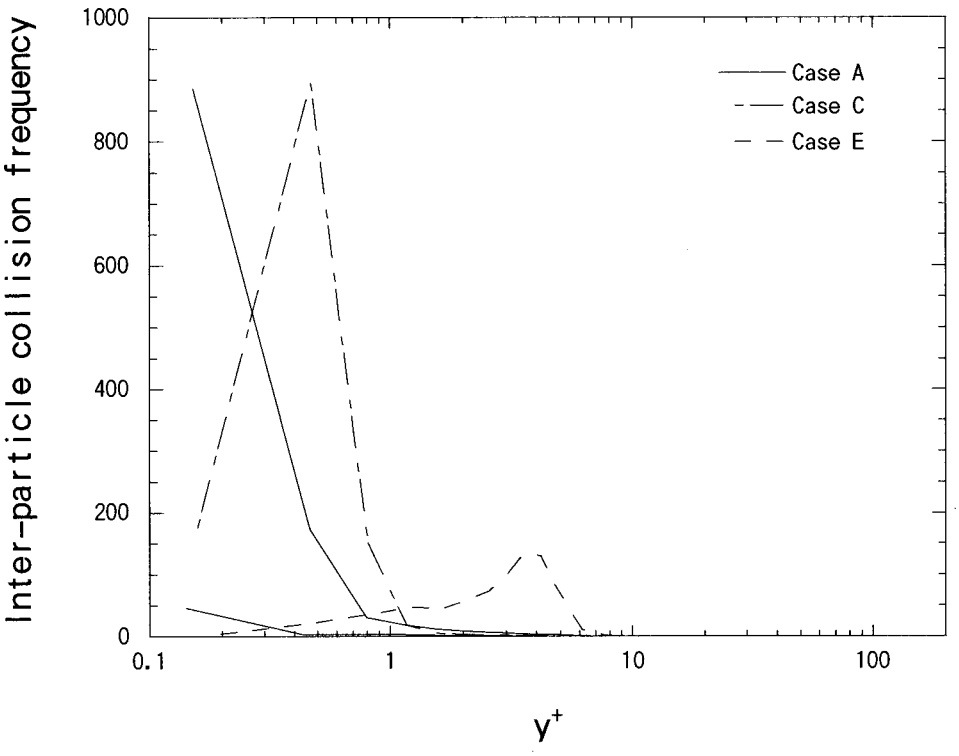

FIG. 13. Mean interparticle collision frequency distribution in wall coordinates.

sidering the interparticle collisions [Fig. 12(a)], more particles tend to concentrate in the vicinity of both surfaces and fewer particles are located slightly away from the surfaces, $y^+>0.3$. On the contrary, for the cases D and F not considering the interparticle collisions, fewer particles tend to concentrate in the vicinity of the pressure surface and more particles are located slightly away from the surface, $y^+>0.65$ for case D and $y^+>5.5$ for case F, respectively. Therefore, the interparticle collisions play a very important role in the rotating system, although the averaged particle volume fractions are very low.

Figure 13 shows the mean interparticle collision frequency based on the average collision frequency in wall coordinates. The peak frequencies occur at different positions for the different particles. Peak frequency values reach 886.0 at $y^+=0.151$ for the case A, and 932.0 at $y^+=0.468$ for the case C, and 119.0 at $y^+=4.17$ for the case E near the pressure surfaces, respectively. Compared with Fig. 12, it is found that the inter-particle collision frequency is proportional to particle density distribution in wall coordinates.

IV. CONCLUSION

This paper provides a numerical investigation of the turbulent rotating channel flows at the Reynolds number $\mathrm{Re}_\tau=u_\tau H/\nu=194$ and the rotation number $\mathrm{Ro}_\tau=\Omega H/u_\tau=0.075$ laden with small particles. Three kinds of particles of different diameters with the same number (156 159 particles) were traced using the deterministic method with two-way coupling. Particle gravity parallel to the spanwise direction and particle volume fractions from $O(10^{-6})$ to $O(10^{-5})$ were considered. A hard-sphere collision model was applied to observe its effects on the turbulence and the preferential concentration of the particles subjected to rotation.

The numerical results from the simulations of the particle-laden flows are analyzed to examine the particle effects on the turbulence. Many particles accumulate in the region near the pressure surface subjected to weak rotation. So, the interparticle collisions are important in the particle-laden rotating channel flows, even at very low averaged particle volume fractions $O(10^{-5})$. It is found that the effect of heavier particles ($\mathrm{St}_\tau>0.1$) and their interparticle collisions near the pressure surface is significantly to modify the turbulence properties, particularly in the near-wall region. The DNS results also show that the effects of the interparticle collisions are to make the lighter particle distributions more even and then suppress the fluid turbulence, and make the heavier particle distributions more uneven and then enhance the fluid turbulence.

We also presented ''snapshots'' of the near-wall particle distribution and obtained the root-mean-square values of particle number per cell to evaluate the intensities of the particle concentrations. The present glass particles ($\mathrm{St}_\tau=0.126$) have strong streaky structures, added hooks with a certain skew angle to the streamwise direction near the pressure surface. Fewer heavier simulated particles ($\mathrm{St}_\tau=0.674$) accumulate in the region very close to the pressure surface due to larger inertia. The well-known low/high-speed streaks close to the boundary are destroyed by the particles subjected to the system rotation when the particles become larger and heavier, and particle volume fraction reaches $O(10^{-5})$.

The numerical experiments reported herein provide information of the fully developed particle-laden rotating channel flows. The DNS results also can provide the database for establishing the subgrid stress modeling in the large eddy simulation of the particle-laden rotating turbulent flows.

ACKNOWLEDGMENTS

The computer code development and simulations were performed on the NEC SX-4 supercomputer at the Computer Center of Osaka University, Japan. The first author is thankful for the financial support for this study by the Japanese Government (Monbusho) scholarship. This research was partially supported by Japan Society for the Promotion of Science, Grant-in-Aid for Scientific Research, No. 11650175.

[1]P. Bradshaw, ''The analogy between streamline curvature and buoyancy in turbulent shear flow,'' J. Fluid Mech. **36**, 177 (1969).
[2]J. P. Johnston, R. M. Halleen, and D. K. Lezius, ''Effects of spanwise rotation on the structure of two-dimensional fully developed turbulent channel flow,'' J. Fluid Mech. **56**, 533 (1972).
[3]D. J. Tritton, ''Stabilization and destabilization of turbulent shear flow in a rotating fluid,'' J. Fluid Mech. **241**, 503 (1992).
[4]C. Cambon, J. P. Benoit, L. Shao, and L. Jacquin, ''Stability analysis and large eddy simulation of rotating turbulence with organized eddies,'' J. Fluid Mech. **278**, 175 (1994).
[5]R. Kristoffersen and H. I. Andersson, ''Direct simulations of low-Reynolds-number turbulent flow in a rotating channel,'' J. Fluid Mech. **256**, 163 (1993).
[6]J. B. McLaughlin, ''Aerosol particle deposition in numerically simulated channel flow,'' Phys. Fluids A **1**, 1211 (1989).
[7]J. W. Brooke, K. Kontomaris, T. J. Hanratty, and J. B. McLaughlin, ''Turbulent deposition and trapping of aerosols at a wall,'' Phys. Fluids A **4**, 825 (1992).
[8]J. W. Brooke, T. J. Hanratty, and J. B. McLaughlin, ''Free-flight mixing and deposition of aerosols,'' Phys. Fluids **6**, 3404 (1994).
[9]S. Pedinotti, G. Mariotti, and S. Banerjee, ''Direct numerical simulation of particle behaviour in the wall region of turbulent flows in horizontal channels,'' Int. J. Multiphase Flow **18**, 927 (1992).
[10]D. W. I. Rouson and J. K. Eaton, ''Direct numerical simulation of turbulent channel flow with immersed particles,'' ASME/FED Numerical Methods in Multiphase Flows, 185 (1994).
[11]K. D. Squires and J. K. Eaton, ''Preferential concentration of particles by turbulence,'' Phys. Fluids A **3**, 1169 (1991).
[12]L.-P. Wang and M. R. Maxey, ''Settling velocity and concentration distribution of heavy particles in homogeneous isotropic turbulence,'' J. Fluid Mech. **256**, 27 (1993).
[13]S. E. Elghobashi and G. C. Truesdell, ''Direct simulation of particle dispersion in decaying isotropic turbulence,'' J. Fluid Mech. **242**, 655 (1992).
[14]W. Ling, J. N. Chung, T. R. Troutt, and C. T. Crowe, ''Direct numerical simulation of a three-dimensional temporal mixing layer with particle dispersion,'' J. Fluid Mech. **358**, 61 (1998).
[15]Y. Pan and S. Banerjee, ''Numerical investigation of the effects of large particles on wall-turbulence,'' Phys. Fluids **9**, 3786 (1997).
[16]L.-P. Wang, A. S. Wexler, and Y. Zhou, ''On the collision rate of small particles in isotropic turbulence. I. Zero-inertia case,'' Phys. Fluids **10**, 266 (1998).
[17]Y. Zhou, A. S. Wexler, and L.-P. Wang, ''On the collision rate of small particles in isotropic turbulence. II. Finite inertia case,'' Phys. Fluids **10**, 1206 (1998).
[18]S. Sundaram and L. R. Collins, ''Collision statistics in an isotropic, particle laden turbulent suspension. I. Direct numerical simulations,'' J. Fluid Mech. **335**, 75 (1997).
[19]P. G. Saffman and J. S. Turner, ''On the collision of drops in turbulent clouds,'' J. Fluid Mech. **1**, 16 (1956).
[20]J. Abrahamson, ''Collision rates of small particles in a vigorously turbulent fluid,'' Chem. Eng. Sci. **30**, 1371 (1975).
[21]S. Sundaram and L. R. Collins, ''A numerical study of the modulation of isotropic turbulence by suspended particles,'' J. Fluid Mech. **379**, 105 (1999).
[22]Y. Yamamoto, T. Tanaka, and Y. Tsuji, ''LES of gas-particle turbulent channel flow (the effect of interparticle collision on structure of particle distribution),'' Proceedings of the 3rd International Conference on Multiphase Flow, 518 (1998).
[23]W. Tabakoff, ''Review-turbomachinery performance deterioration exposed to solid particulates environment,'' ASME J. Fluids Eng. **106**, 125 (1984).
[24]Y.-K. Pan, T. Tanaka, and Y. Tsuji, ''Large-eddy simulation of particle-laden rotating channel flows,'' ASME FEDSM2000-11144 (Boston, 2000).
[25]P. R. Spalart, R. D. Moser, and M. M. Rogers, ''Spectral methods for the Navier–Stokes equations with one infinite and two periodic directions,'' J. Comput. Phys. **96**, 297 (1991).
[26]J. Kim and P. Moin, ''Application of a fractional-step method to incompressible Navier–Stokes equations,'' J. Comput. Phys. **59**, 308 (1985).
[27]M. R. Maxey and J. J. Riley, ''Equation of motion for a small rigid sphere in nonuniform flow,'' Phys. Fluids **26**, 883 (1983).
[28]L. Schiller and A. Naumann, ''Uber die grundlegenden berechnungen bei der schwerkraftaufbereitung,'' Verh. Dtsch. Ing. **77**, 318 (1933).
[29]S. I. Rubinow and J. B. Keller, ''The transverse force on a spinning sphere moving in a viscous fluid,'' J. Fluid Mech. **11**, 447 (1961).
[30]Y. Tsuji, *Pneumatic Conveying* (Nikkann, Kogyo, 1984) (in Japanese).
[31]P. G. Saffman, ''The lift on a small sphere in a slow shear flow,'' J. Fluid Mech. **22**, 385 (1965).
[32]P. G. Saffman, Corrigendum to ''The lift on a small sphere in a slow shear flow,'' J. Fluid Mech. **31**, 624 (1968).
[33]D. Hall, ''Measurements of the mean force on a particle near a boundary in turbulent flow,'' J. Fluid Mech. **187**, 451 (1988).
[34]T. Tanaka and Y. Tsuji, ''Numerical simulation of gas-solid two-phase flow in a vertical pipe: one the effect of inter-particle collision,'' ASME/FED Gas–Solid Flows, 123 (1991).
[35]S. C. R. Dennis, S. N. Singh, and D. B. Ingham, ''The steady flow due to a rotating sphere at low and moderate Reynolds number,'' J. Fluid Mech. **101**, 257 (1980).
[36]H. Takagi, ''Viscous flow induced by slow rotation of a sphere,'' J. Phys. Soc. Jpn. **42**, 319 (1977).
[37]J. Kim, P. Moin, and R. Moser, ''Turbulence statistics in fully developed channel flow at low Reynolds number,'' J. Fluid Mech. **177**, 133 (1987).
[38]Y.-K. Pan, T. Tanaka, and Y. Tsuji, ''Numerical study of particle-laden rotating turbulence,'' 4th International Conference on Multiphase Flow (ICMF-2001), New Orleans, 2001.